The R-domain: Identification of an N-terminal region of the $\alpha_2\delta$-1 subunit which is necessary and sufficient for its effects on $Ca_v2.2$ calcium currents

Lele Song, Italo A. Espinoza-Fuenzalida, Sarah Etheridge, Owen T. Jones, Elizabeth M. Fitzgerald

*Faculty of Life Sciences, The University of Manchester, Michael Smith Building, Manchester, M13 9PT, UK.

*Corresponding Author

Dr. Elizabeth M. Fitzgerald

A1022 Michael Smith Building,

Manchester, U.K.

M13 9PT

Email: Elizabeth.m.fitzgerald@manchester.ac.uk

Tel: +44 (0)161 275 5495/5604

Fax: +44 (0)161 275 5600

Abstract

Voltage-gated calcium channels (Ca_v) and their associated proteins are pivotal signalling complexes in excitable cell physiology. In nerves and muscle, Ca_v tailor calcium influx to processes including neurotransmission, muscle contraction and gene expression. Ca_v comprise a pore-forming α_1 and modulatory β and $\alpha_2\delta$ subunits – the latter targeted by anti-epileptic and anti-nociceptive gabapentinoid drugs. However, the mechanisms of gabapentinoid action are unclear, not least because detailed structure-function mapping of the $\alpha_2\delta$ subunit remains lacking. Using molecular biology and electrophysiological approaches we have conducted the first systematic mapping of $\alpha_2\delta$ subunit structure-function. We generated a series of cDNA constructs encoding chimera, from which successive amino acids from the rat $\alpha_2\delta$-1 subunit were incorporated into a Type 1 reporter protein – PIN-G, to produce sequential extensions from the transmembrane (TM) region towards the N-terminus. By successive insertion of a TGA stop codon, a further series of N- to C-terminal extension constructs lacking the TM region, were also generated. Using this approach we have defined the minimal region of $\alpha_2\delta$-1 - we term the R-domain (Rd) that appears to contain all the machinery necessary to support the electrophysiological and trafficking effects of $\alpha_2\delta$-1 on Ca_v. Structural algorithms predict that Rd is conserved across all four $\alpha_2\delta$ subunits, including RNA splice variants, and irrespective of phyla and taxa. We suggest, therefore, that Rd likely constitutes the major locus for physical interaction with the α_1 subunit and may provide a target for novel Ca_v therapeutics.

1. INTRODUCTION

Voltage-gated calcium channels (Ca_v) couple changes in membrane potential to the influx of Ca^{2+}, a pivotal second messenger in events such as muscle contraction, neurosecretion, neurotransmission and gene expression [1]. Unsurprisingly, Ca_v malfunction causes numerous conditions such as pain, epilepsy and cardiovascular disease in humans and other animals [2].

Ca_v are multi-subunit protein complexes composed of a pore-forming α_1 and (in high voltage-activated Ca_v1 and Ca_v2 channels), also regulatory β and $\alpha_2\delta$ subunits, in a 1:1:1 stoichiometry. To date, 10 α_1, 4 β and 4 $\alpha_2\delta$ subunits have been identified; many with multiple splice variants that are differentially expressed according to tissue and stage of development [1]. The association of β and $\alpha_2\delta$ subunits with α_1 serves two main roles: first, to modify the biophysical properties of Ca_v and thus, how much calcium enters a cell and second, to enhance Ca_v cell surface expression [1, 3]. While structure-function studies have revealed much about how and where auxiliary β subunits interact with the α_1 [3, 4, 5, 6], detailed structure-function mapping of the $\alpha_2\delta$ subunit has remained elusive.

Clinically, $\alpha_2\delta$ subunits are implicated in a growing number of pathological conditions, including epilepsy, pain, and cancer [7-10]. Moreover, $\alpha_2\delta$-1 and -2 are the primary targets of the anti-convulsant and anti-nociceptive gabapentinoid drugs. Gabapentinoids act upon Ca_v to reduce neurotransmitter release and thus nerve excitability, but how they do this remains unclear [11]. Furthermore, whilst these drugs are highly effective and clinically safe in many patients, in others their benefits are severely limited [12, 13]. Detailed mapping of the structure and function of $\alpha_2\delta$ subunits is, thus, fundamental not only to understanding the physiology of Ca_v but also for improving Ca_v pharmacology [14].

The $\alpha_2\delta$ subunit is translated as a single polypeptide which undergoes cleavage into a large α_2 and small δ polypeptides [11, 15]. Both subunits are then re-associated via disulphide bonds and subject to glycosylation to yield the mature $\alpha_2\delta$ subunit [11, 15, 16]. Structurally, all four $\alpha_2\delta$ subunits share a similar topology: a large extracellular α_2 polypeptide tethered to the cell surface via its associated δ subunit [17, 18]. Electrophysiological and biochemical studies indicate the α_2 polypeptide promotes surface expression and modulates the biophysical properties of Ca_v [19, 20, 21, 22]. The δ subunit has also been suggested to influence the biophysical properties of Ca_v [20]. However more recently, expression of the extracellular regions of $\alpha_2\delta$ (minus TM δ) has been reported to support Ca_v currents, thus calling into question the role of the δ subunit [16]. Within α_2, are domains found in non-calcium channel-associated proteins, namely a Von Willebrand Factor A (VWA) and Cache domains [23,24,].

In $\alpha_2\delta$-1 and -2 isoforms, the VWA domain contains a metal ion adhesion site (MIDAS) motif. In heterologous expression systems, the MIDAS enhances $\alpha_2\delta$-mediated trafficking of Ca_v to the cells surface [25]. However, its role in the function native neuronal Ca_v is less clear [26]. The N-terminal region of $\alpha_2\delta$-1 and -2 VWA domains also contain key residues for gabapentinoid binding [15, 27, 28]. Whilst the mode of action of gabapentinoids is controversial, disruption of this principal gabapentin-binding site causes modest (20-30%) reduction of Ca_v current, suggesting its integrity is critical for $\alpha_2\delta$ function [15,27,28]. The VWA domain has also been identified as the receptor for thrombospondin (TSP), an extracellular matrix protein [29]. Gabapentin is suggested to disrupt the TSP/$\alpha_2\delta$-1 interaction, thereby inhibiting synaptogenesis [29]. Thus, in $\alpha_2\delta$ subunits, the VWA domain appears to fulfil similar protein interaction and possibly conformational "switch" roles to those it has in other cell surface proteins, including integrins [23]. Cache domains are found in proteins that sense small molecule ligands, notably bacterial chemotaxis proteins [24]. Whilst the ligands for the $\alpha_2\delta$ Cache domain have not been identified, residues proximal to it are reportedly involved in gabapentin-binding [30].

More surprising, given its functional importance, is that the regions of $\alpha_2\delta$ that mediate its interaction with α_1 subunits are currently unknown. There is evidence that transmembrane domains II and III of the α_1 subunit may be involved in binding $\alpha_2\delta$; thus multiple contact sites may exist in the interacting partners [20, 31]. To begin addressing these critical issues, we have combined molecular and electrophysiological approaches to conduct the most detailed structure-function mapping of $\alpha_2\delta$ to date. We generated a series of cDNA constructs encoding chimera in which the extracellular head of a similar Type 1 protein – PIN-G [18, 32] was fused to successive polypeptides and amino acids of the rat $\alpha_2\delta$-1 sequence. Using this approach we have identified the minimal region of $\alpha_2\delta$ - the R-domain (Rd) - that is both necessary and sufficient to impart the primary functional effects of $\alpha_2\delta$ on $Ca_v2.2$, the N-type channel. Thus, we suggest that Rd contains all the machinery required to support Ca_v kinetics and expression. Moreover, since the Rd is highly conserved in all known subtypes, we suggest that Rd likely represents the primary locus for physical interaction with Ca_v α_1 subunits and may provide a target for development of novel therapeutics targeting Ca_v.

2. METHODS AND MATERIALS

2.1 Reagents

Constructs encoding rabbit $Ca_V2.2$ (D14157), rat $Ca_v\beta_{1b}$ (X61394) and GFP (U73901, mut-3 variant) cloned into the mammalian expression vector pMT2, were provided by A.C. Dolphin (University College

London, UK). The construct encoding wild type rat $Ca_v\alpha_2\delta$-1 (neuronal splice variant NM_012919.2) cloned into pcDNA3.1 (Invitrogen) was supplied by T.P. Snutch (Univ. British Columbia, Canada). The PIN-G reporter construct (Genbank: AY841887) was developed by O.T. Jones [32] and is available upon request. All other reagents were obtained from Sigma-Aldrich, UK, unless stated otherwise.

2.2 Molecular biology

All PIN constructs were prepared through the sequential addition, removal or replacement [33] of requisite $\alpha_2\delta$-1 sequences into PIN-G, containing both Green fluorescent protein (GFP) and Haemagglutinin (HA) tags [18]. For electrophysiology, equivalent constructs lacking the GFP tag were generated to avoid any adverse effects on current properties [18]. Thus, the PIN "head" (Fig. 1A) of each construct corresponds to the N-terminal region of PIN-G, containing a signal peptide, an exofacial HA tag and short linker [32]. PIN chimera containing the PIN "head" fused to the $\alpha_2\delta$-1 sequences specified (Figs. 1, 2 and 3), were constructed through the initial replacement of the sequence encoding the PIN-G transmembrane and intracellular region (residues 327-370) with that encoding WT $\alpha_2\delta$-1 residues 1061-1091 (i.e. δTM , Fig. 1A), to yield PIN-TM. All further chimera were generated by step-wise insertion of the adjacent $\alpha_2\delta$ residues specified. Throughout, mutagenesis was done using the QuikChange™ Lightning kit (Agilent Technologies, UK) and mutagenic megaprimers prepared by PCR. The fidelity of each construct was confirmed by in-house sequencing (see Figs. 1, 2 and 3 for chimera junctions). Western blotting was used to confirm that all the resultant proteins were of the expected size (data not shown).

2.3 Cell culture and transient transfection

Culture and transient transfection of COS-7 cells (European Cell Culture Collection, Health Protection Agency, U.K.), were carried out as described in Robinson et al. [18,34]. Transient transfection was performed in serum-free DMEM, (cell confluency 60-70%) using FuGene 6 (Roche Diagnostics, U.K.) at a total DNA:reagent ratio of 1:3 (w/v) and a $Ca_v2.2$:β_{1b}:PIN-$\alpha_2\delta$:mut3-GFP-pMT2 cDNA mass ratio of 3:1:1:0.2, respectively (1 µg total DNA/35mm dish). When PIN-$\alpha_2\delta$ was omitted the mass ratio was maintained by substitution with pcDNA3.1. After transfection, cells were maintained for 48 h in complete medium prior to conducting electrophysiological experiments.

2.4 Whole-cell patch-clamp electrophysiology

Electrophysiological recordings of inward barium currents were made from green fluorescent COS-7 cells, using the whole-cell configuration of the patch clamp technique, as described previously [18]. The internal solution contained (mM): caesium aspartate 140.0; EGTA 5.0; $MgCl_2$ 2.0; $CaCl_2$ 0.1; Hepes 20.0; K_2ATP 1.0; adjusted to pH 7.2 with CsOH and 310 mOsm l^{-1} with sucrose. The external solution contained (mM): TEABr 160.0; $MgCl_2$ 1.0; KCl 5.0; $NaHCO_3$ 1.0; Hepes 10.0; glucose 4.0; $BaCl_2$ 10; adjusted to pH 7.4 with Tris-base and to 320 mOsm l^{-1} with sucrose. Currents were recorded using an Axopatch 200B amplifier (Molecular Devices, Palo Alto, CA, USA), were filtered at 2 Hz and digitized at 2-44 kHz using a Digidata 1440A A/D converter (Molecular Devices). Standard current-voltage protocols comprised 200 ms sweeps from a holding potential, V_h of -80 mV to command voltages of -30 to +65 mV in 5 mV steps. Current density-voltage (*I-V*) relationships for individual cells were fitted with a Boltzmann function:
$I = (g(V-V_{rev}))/(1+\exp(-(V-V_{50,act})/k))$, where, V_{rev} is the reversal potential, $V_{50,act}$ is the voltage for half maximal activation of current, g is the conductance, and k is the slope factor.
Steady-state inactivation curves were obtained from individual cells using 100 ms duration test pulses to 20 mV, preceded by a 5 s pre-pulse to the potential given (-90 to +30 mV), from V_h –80 mV. Peak current values were normalized to I_{max} and the curves fitted with the following Boltzmann function:
$I/I_{max} = 1/(1+\exp(V_t-V_{50,inact})/k))$, where, I_{max} is the maximum peak current, $V_{50,inact}$ is the midpoint of voltage-dependent inactivation and k is the slope factor.
Data acquisition and analysis were performed using pCLAMP software (version 10, Molecular Devices) and Origin (v 7.0, Microcal, Northampton, MA, USA).

2.5 Western blot and PNGase-F assay

COS-7 cells were grown in DMEM (Sigma) supplemented with 5% FBS (Gibco, Life Sciences) for each condition and were harvested 48 hours after transfection. They were washed with ice-cold PBS- and lysed with RIPA buffer (Sigma-Aldrich), plus protease inhibitors (Complete protease inhibitor kit, Roche). The cell extract was incubated on ice for 15 min and then centrifuged at maximum speed (~13000 rpm) for 30 min. The supernatant was collected and the pellet discarded. The protein concentration was determined by Pierce BCA Protein Assay kit (Thermo Scientific, Rockford, USA). For the PNGase-F assay, 20 µg of protein were used, following the manufacturer's instructions (PNGAse-F assay, New England Biolabs, UK). Briefly, samples were boiled for 10 min at 100^{o}C with 1x Glycoprotein Denaturation buffer (5% SDS, 5% DTT), and then added 1x G7 Reaction buffer, 1% NP-40 and 1µl of PNGase-F. The mix was incubated 60 min at 37 ^{o}C. For the Western blot, 20 µg of sample were loaded per well, using 6x loading buffer (Life Technologies, Carlsbad, CA, USA) with or without DTT, and separated using a Bolt™ electrophoresis system (Life Technologies, Carlsbad, CA, USA). Proteins were transferred using an iBlot®

2 Dry Blotting System (Life Technologies, Carlsbad, CA, USA) onto nitrocellulose membranes, blocked with 5% non-fat milk (Biorad) in 0.2% Tween-20 (Sigma) in TBS (TBS-T), and incubated for 1 h with the primary antibody (Anti-HA, 1:5000; Sigma). After three washes with 0.2% TBS-T, membranes were incubated with the secondary antibody (anti-mouse, 1:5000; Biorad) for 1 h and then washed three times. The membranes were developed using the ECL Western Blotting Substrate (Promega, USA) into Amersham Hyperfilm™ (GE Healthcare, UK).

2.6 Data analysis

All data are presented as the mean ± standard error of the mean (S.E.M) for *n* trials. Statistical analysis was carried out by One-way ANOVA followed by Least Significant Difference *post hoc* correction, using 95% confidence limits (Statistica, v 4.5; Statsoft Inc).

3. RESULTS

3.1 Initial mapping of $\alpha_2\delta$-1 functional domains

The classical hallmarks of $\alpha_2\delta$-mediated Ca_v current modulation include, enhanced current density (typically 3- to 5-fold), a hyperpolarizing shift in voltage-dependence of activation and increased voltage-dependent inactivation of current [9]. We recently reported that insertion of the N-terminal 'head' (i.e. HA tag and spacer sequence) of a functionally inert Type-1 TM protein reporter - PIN-G - into the sequence encoding mature rat $\alpha_2\delta$-1, yields a chimera (PIN-$\alpha_2\delta$;[32]) whose function mirrors that of wild type (WT) $\alpha_2\delta$-1 [18,34]. As predicted, here too the co-expression of PIN-$\alpha_2\delta$ with $Ca_v2.2/\beta_{1b}$ increased maximum peak current density, I_{max} (Fig. 1, Table 1), hyperpolarized the voltage-dependence of activation ($V_{50,act}$), reduced the slope factor, *k* (increased voltage sensitivity) and enhanced current inactivation (measured as percent inactivation after 500 ms, % Δ inact).

To determine which functional domains of $\alpha_2\delta$-1 were responsible for these effects, we initially designed several PIN-$\alpha_2\delta$-1 chimera, starting from the transmembrane exofacial (TM) region of δ, and building up towards the N-terminal (Fig. 1A,B): PIN-TM, PIN-δ, PIN-Linker, PIN-VGCC, PIN-Cache and PIN-VWA. In agreement with other workers, PIN-TM and PIN-δ had no effects on Ca_v current (Fig. 1C-E) [19, 20, 21, 22]. Based on the location of the disulphide bond between α_2 (VWA domain) and δ [16], PIN-Linker, -VGCC and -Cache are predicted to be uncoupled from δ and thus potentially secretable [22]. Despite the fact that α_2 alone has been shown to support Ca_v current [22], PIN-Linker, -VGCC, -Cache were also unable to support any $\alpha_2\delta$-mediated effects on $Ca_v2.2/\beta_{1b}$ current. Similarly, PIN-VWA, predicted to be

membrane-anchored due to the presence of the disulphide bond [16], was also without any effect on $Ca_v2.2/\beta_{1b}$ current. Comparison of PIN-$\alpha_2\delta$, PIN-VWA and PIN-Cache constructs, showed similar expression levels and a similar level of N-linked glycosylation, as determined by treatment with PNGase-F (Fig. 1B, inset). Together, these data suggest that addition of the final N-terminal region – hereafter termed, "R" domain (Rd, amino acids 26-230) – is essential for $\alpha_2\delta$ function.

3.2 Functional mapping of the N-terminal R domain of $\alpha_2\delta$-1

Having established the need for Rd, we next mapped the region(s) that might be involved in mediating $\alpha_2\delta$ function. Initially, we generated two further PIN-chimera: PIN-C1 and PIN-B1 (Fig. 2A,B). However, neither construct restored the effects of full length PIN-$\alpha_2\delta$ on $Ca_v2.2/\beta_{1b}$ currents (Fig. 2C,D), indicating that region Rd-A (residues 26-117) is necessary for the functional modulation of channels by $\alpha_2\delta$.

Multiple sequence alignments revealed a high degree of sequence conservation within Rd-A across a total of 109 available full length Rd sequences from species spanning the evolutionary spectrum, including all four human $\alpha_2\delta$ subunits (Supp. Fig. S1). Computer-aided modelling of Rd structure predicted that Rd-A contains two putative α-helices (Supp. Fig. S2) – which, we hypothesized, could play a role in mediating the interaction of $\alpha_2\delta$ with the $Ca_v\alpha_1$ subunit. Thus, we generated three further chimera: PIN-A4, PIN-A3 and PIN-A2 (Fig. 2A,B) to bisect the predicted α-helices. PIN-A4 was unable to support normal $\alpha_2\delta$ function but the addition of Rd-A3 (PIN-A3) induced a 4-fold increase in I_{max} (Fig. 2C,D; Table 1), significant hyperpolarization of $V_{50,act}$ (Fig. 2C,D; Table 1) and enhanced voltage sensitivity (reduced *k*; Table 1). However, % Δ inact of PIN-A3 currents was the same as in the absence of $\alpha_2\delta$ and only upon further addition of region Rd-A2 (PIN-A2), was normal inactivation restored (Fig. 2D; Table 1). The addition of Rd-A2 also further increased I_{max} (5-fold, Fig. 2; Table 1), such that $Ca_v2.2/\beta_{1b}$/PIN-A2 currents were indistinguishable from those with full length PIN-$\alpha_2\delta$. Thus, whilst Rd-A3 appears primarily responsible for up-regulation of current density and shifts in the *I-V* relationship, addition of Rd-A2 appears necessary for normal inactivation. Together, Rd-A3 and Rd-A2 span the two predicted α-helices, with Rd-A3 also encompassing an intervening "loop" region (Supp. Fig. S2). Thus, we suggest that the integrity of the two putative α-helices within Rd-A is critical for normal functioning of $\alpha_2\delta$. Further functional mapping confirmed that the presence of Rd-A3 as a whole is essential to impart $\alpha_2\delta$-mediated modulation of Ca_v (Figs. 2, 3 and Table 1). However, the addition of Rd-dA3 only (residues 86-90) is sufficient for the $\alpha_2\delta$-mediated shift in $V_{50,act}$, implying that this region is important in defining the threshold of Ca_v activation.

3.4 Is Rd-A alone sufficient for modulation of current by $\alpha_2\delta$?

Given that expression of the EC regions of $\alpha_2\delta$ alone are sufficient to support Ca_v currents [22], we next asked whether expression of Rd-A alone could promote $\alpha_2\delta$ function. To address this, a stop codon (TGA) was inserted immediately after Rd-A (residues 26-117) to produce a truncated PIN-RdA construct (Fig. 3A). PIN-RdA, however, failed to elicit any of the electrophysiological effects associated with full length $\alpha_2\delta$ (Fig. 3B,C; Table 1). Similarly, constructs in which the stop codon was inserted at successively extended positions from Rd-A through to Rd; PIN-RdB1, PIN-RdB2, PIN-RdC1 (Fig.3A), also failed to elicit any modulation of current (Fig. 3B,C; Table 1). However, co-expression of the full R domain (PIN-Rd) was sufficient to restore all the hallmarks of $\alpha_2\delta$-mediated current modulation, including an increase in current density comparable to that seen with PIN-$\alpha_2\delta$ (Fig. 3B,C; Table 1). This suggests that Rd contains all the machinery necessary for $\alpha_2\delta$-dependent modulation of Ca_v. Moreover, both the N- (Rd-A) and C-terminal (Rd-C2) regions of Rd are required to impart these $\alpha_2\delta$-dependent effects on Ca_v current.

Western blotting confirmed the presence of PIN-Rd at the predicted size of approximately 50kDa (GFP- and HA-tagged). Treatment with PNGase-F indicated that the protein is glycosylated, as predicted on the basis that N-linked glycosylation sites, N163 and N184, known to be critical for Ca_v current enhancement, are located within Rd (Fig. 3C, inset) [16].

Having established that PIN-Rd was correctly processed, we further examined region Rd-C. Multiple sequence alignments revealed a high degree of sequence conservation across all Rds tested, including an 11 amino acid sequence between residues 200-210 (Supp. Fig. S1). Deletion of this C2 region from either full length $\alpha_2\delta$ (PIN-$\alpha_2\delta$-Δ11) or Rd (PIN-Rd-Δ11), completely abolished the effects of $\alpha_2\delta$ (and Rd) on I_{max}, $V_{50,act}$ and k (Fig. 3D,E; Table 1). However, % Δ inact was unaffected, (Fig. 3D,E; Table 1). The 11 residue C2 sequence contains a conserved tryptophan (W205), present in >99% of all documented $\alpha_2\delta$ isoforms (Supp. Fig. S1). Remarkably, substitution of W205 with alanine (PIN-Rd-W205A) proved sufficient to abolish all the classical hallmarks of $\alpha_2\delta$-mediated current modulation, with the exception of enhanced inactivation. Thus, Rd-C2 and more specifically W205, appears essential for $\alpha_2\delta$-mediated modulation of Ca_v current. However, the additional presence of the N-terminal Rd-A region is also necessary for the regulation of current inactivation and hence full function of Rd/$\alpha_2\delta$.

3.5 Rd structure prediction

To gain insights into how Rd might operate, we compared 3D models generated from divergent sequences through *ab initio* computer modelling. Using the QUARK algorithm, which constructs 3D

models from sequence fragments using replica-exchange Monte Carlo simulation guided by an atomic-level, knowledge-based, force field [36,37], all four human Rds are predicted to adopt very similar folded structures (Supp. Fig. S2A-D). In all sequences, Rd-A comprises two anti-parallel α-helices adopting a partially coiled-coil structure. Rd-C contains a single α-helix in region C1 plus a 16 residue "tongue" formed between highly conserved prolines (rat Rd-1: P180 and P198) in region C2. Comparison of the wild-type Rd-1 (Fig. 4A) versus the mutant Rd-1-W205A (Fig. 4B), indicates a vertical displacement of Rd-B and inversion of the entire Rd-C region. Thus, W205 may play an important structural role, possibly as part of a conformational "switch" mechanism. Whilst such models clearly require experimental validation, their essential features fit remarkably well with our structure-function data.

4. DISCUSSION

In this study, we have identified residues 26-230 in the rat $\alpha_2\delta$-1 sequence (representing the first 205 amino acids of the mature α_2 polypeptide and just 19% of mature $\alpha_2\delta$-1), termed Rd, as being the minimal sequence required to induce $\alpha_2\delta$-1 modulation of Ca_v current density and biophysical properties. Although Rd functionality appears to require both the N and C terminal regions (Rd-A, residues 26-117 and Rd-C, residues 165-230), further mapping reveals that effects on channel gating only emerge as residues are added progressively from position 117 to 26. Thus, Rd-A contributes significantly to the $\alpha_2\delta$-α_1 interaction. Since Rd-A is predicted to contain two putative α-helices (Supp. Fig. S2), it is conceivable that successive addition of N-terminal residues proximal to position 117, progressively stabilize the conformation/orientation of Rd-A such that full $\alpha_2\delta$-1-mediated modulation of current can occur.

In addition to Rd-A, we also identified the need for a highly conserved tryptophan residue (W205, $\alpha_2\delta$-1) located within Rd-C2, that is found in nearly all documented $\alpha_2\delta$ subunits (Supp. Figs. S1, S2). Interestingly, the Rd-C regions are not only highly conserved amongst $\alpha_2\delta$ subunits, but represent a poorly characterized module found in proteins containing VWA (and Cache) domains, referred to as the N-terminal VWA domain (N-VWA) (pfAM PF08399, http://pfam.sanger.ac.uk). Nevertheless, while it appears to be a critical feature of Rd, the N-VWA domain is just one component, and our data indicate that additional regions, Rd-B and -A, are absolute requirements for Ca_v current enhancement. Moreover, functionality of Rd alone requires Rd-C (i.e. N-VWA) even in the absence of the adjacent VWA domain. Thus, Rd can be viewed as an integral unit that may have evolved on a platform – N-VWA – to which its Ca_v-specific functions have been attached.

Our identification of Rd as the minimal region supporting $\alpha_2\delta$-mediated modulation of Ca_v is consistent with other studies which have attributed enhanced Ca_v surface expression and biophysical modification to the α_2 polypeptide [19-22]. Notably, our data support the recent finding, that the EC regions of $\alpha_2\delta$, untethered from the membrane, can support Ca_v current enhancement [22]. Also, deletion of amino acids 28-184 of rat brain $\alpha_2\delta_b$ (approximating Rd) was reported to abolish its ability to enhance $Ca_v2.1/\beta_4$ current [19]. The VWA domain and, more specifically, its constituent MIDAS motif, has also been suggested to promote $\alpha_2\delta$-2-induced Ca_v current enhancement [25], although this may not be the case in native neurons [26]. More recently, a region downstream of VWA has been suggested to form part of the site of interaction with the α_1 subunit [31]. Whilst our functional mapping of $\alpha_2\delta$-1 provides no evidence that addition of sequences between δ-TM and α_2-VWA is sufficient to restore the functional effects of full length $\alpha_2\delta$-1, this does not rule out their physiological importance in full length $\alpha_2\delta$-1 of native cells. Rather, since Rd appears both necessary and sufficient to replicate the effects of $\alpha_2\delta$-1, we envisage that other regions of $\alpha_2\delta$ likely contribute intra- and/or inter-molecular interactions that modify the conformation or orientation of Rd, and hence its association with, or affinity for, the α_1 subunit. In this regard, it is notable that gabapentinoid (GBP) drugs target an RRR motif 33 amino acids downstream of W205 at the boundary between Rd and VWA of $\alpha_2\delta$-1, [38,39]. Thus, GBP-binding may disrupt the orientation of Rd and hence its association with α_1.

The functional characteristics of $Ca_v2.2/\beta_{1b}$ channels co-expressed with Rd - which is potentially secretable [22] - or full length, membrane-associated PIN-$\alpha_2\delta$, are indistinguishable, consistent with maintenance of Rd-α_1 subunit interactions at the cell surface where Ca_v function is detected. Nevertheless, Rd-α_1 interactions could occur at any stage from assembly and surface expression to degradation of Ca_v. The most profound effect of $\alpha_2\delta$ on Ca_v current enhancement is thought primarily to reflect an increase in the anterograde trafficking of Ca_v complexes and/or a decrease in their internalization (stabilization) [11]. However, since Rd lacks those downstream VWA and δ sequences that facilitate stabilization (via ECM and raft interactions, respectively) [18, 29], Rd is perhaps more likely to enhance anterograde Ca_v trafficking, possibly by masking ER-retention determinants in the α_1 pore. This would certainly be consistent with suggestions of other workers that current enhancement primarily involves increased surface expression of Ca_v and that association of α_1 and $\alpha_2\delta$ subunits likely occurs within the secretory pathway, rather than at the cell surface [11, 31].

However, effects on channel gating, particularly the marked hyperpolarization of activation threshold, may also contribute to current enhancement. For example, although $Ca_v1.2$ current is enhanced in the

presence of $\alpha_2\delta$ [19], the surface expression of $Ca_v1.2/\beta$ complexes are not always increased [40]. We also have observed that $\alpha_2\delta$ fails to increase surface expression of $Ca_v1.2$ subunit (I. Espinoza-Fuenzalida and E.M. Fitzgerald, unpublished observations), contrary to its effects on $Ca_v2.2$ [18, 31, 34]. Further work is clearly necessary to determine the precise mechanism(s) of $\alpha_2\delta$-mediated current enhancement. Nonetheless, it is tempting to speculate that $\alpha_2\delta$s may differentially regulate Ca_v, with effects on trafficking (e.g. $Ca_v2.2/2.1$) and/or gating (e.g. $Ca_v1.2$) dependent upon the specific Ca_v α_1 isoform associated. Notably, L-type agonists such as BayK8644 can elicit large gating-mediated increases in $Ca_v1.2$ current density (3 to 5-fold) which are comparable to the effect of $\alpha_2\delta$ co-expression [41,42]. However, the extent of any such isoform-specific effects will need to be clearly established. Despite the strong underlying conservation in the predicted structures of all Rds (Supp. Fig. 2), there is divergence within the underlying Rd sequences, particularly within the Rd-B and -A regions. This may be sufficient to accommodate specificity in α_1-Rd interactions and hence differential regulation of discrete Ca_v. The conserved structural features, suggesting similar modes of action, combined with diversity within the Rd-B and -A regions suggests that selective Rd-α_1 interactions could potentially be exploited for the development of novel therapeutics for a range of disorders including pain, epilepsy, schizophrenia and cardiac arrhythmias [14, 44, 45].

Precisely how Rd operates is uncertain. Based on our mutation studies and computer modelling, the Rd may contain a cavity into which a polypeptide ligand, e.g. from Domain II or III, could dock [20,31]. Since Rd-B is poorly conserved, $Ca_v\alpha_1$ docking sites are perhaps more likely to lie within Rd-A and -C regions, with their accessibility governed by the adjacent VWA domain. Finally, the question arises: if the R domain contains all the machinery required to support Ca_v kinetics and surface expression, what does the rest of the $\alpha_2\delta$ subunit do? Based on recent data, the answer is likely to be three-fold: first, to modulate the Rd-$Ca_v\alpha_1$ interaction, second, to localize the Ca_v complex at sites of cell-cell interaction and third, to concentrate Ca_vs into lipid rafts [18,34]. Overall, we suggest that the R domain represents a critical locus for $\alpha_2\delta$-mediated modulatory, pharmacological and cell biological functions on Ca_vs.

Author contributions

Experiments were conceived and designed by EF, OJ, LS. Experimental work was performed by LS, IE-F and SE. Data were analyzed by LS, IE-F, OJ, EF. The paper was written by EF and OJ.

CONFLICT OF INTEREST

There are no conflicts of interest

ACKNOWLEDGEMENTS

This work was funded by the Medical Research Council, UK (Project Grant I.D. 81568 to EF and OJ) and Becas Chile-CONICYT (PhD Scholarship to IE-F).

REFERENCES

[1] Catterall, W.A., Perez-Reyes, E., Snutch, T.P., Striessnig, J. International Union of Pharmacology XLVIII Nomenclature and structure-function relationships of voltage-gated calcium channels. *Pharmacol Rev,* **2005***, 57*, 411-425.

[2] Striessnig, J., Koschak, A. Exploring the function and pharmacotherapeutic potential of voltage-gated Ca^{2+} channels with gene knockout models. *Channels (Austin),* **2008**, *2*, 233-251.

[3] Dolphin, A.C. Calcium channel diversity: multiple roles of calcium channel subunits. *Curr Opin Neurobiol,* **2009**, *19*, 237-244

[4] Richards, M.W., Butcher, A.J., Dolphin, A.C. Ca^{2+} channel beta subunits: structural insights AID our understanding. *Trends Pharmacol Sci*, **2004**, *25*, 626-632.

[5] Chen, Y., Li, M.H., Zhang, Y., He, L.L., Yamada, Y., Fitzmaurice, A., Shen, Y., Zhang, H., Tong, L., Yang, J. Structural basis of the alpha1-beta subunit interaction of voltage-gated Ca^{2+} channels. *Nature,* **2004**, *429*, 675-680.

[6] Van Petegem, F., Clark, K.A., Chatelain, F.C., Minor, D.L. Structure of a complex between a voltage-gated calcium channel beta-subunit and an alpha-subunit domain. *Nature*, **2004**, *429*, 671-675.

[7] Carboni, G.L., Gao, B., Nishizaki, M., Xu, K., Minna, J.D., Roth, J.A., Ji, L. CACNA2D2-mediated apoptosis in NSCLC cells is associated with alterations of the intracellular calcium signaling and disruption of mitochondria membrane integrity. *Oncogene*, **2003**, *22*, 615-626.

[8] Brodbeck, J., Davies, A., Courtney, J-M., Meir, A., Balaguero, N., Canti, C., Moss, F.J., Page, K.M., Pratt, W.S., Hunt, S.P., Barclay, J., Rees, M., Dolphin, A.C. The ducky mutation in Cacna2d2 results in altered Purkinje cell morphology and is associated with the expression of a truncated alpha2delta-2 protein with abnormal function. *J Biol Chem*, **2002**,*277*, 7684-7693.

[9] Newton, R.A., Bingham, S., Case, P.C., Sanger, G.L., Lawson, S.N. Dorsal root ganglion neurons show increased expression of the calcium channel alpha2delta-1 subunit following partial sciatic nerve injury. *Brain Res Mol Brain Res*, **2001**, *95*, 1-8.

[10]Luo, Z.D., Chaplan, S.R., Huguera, E.S., Sorkin, L.S., Stauderman, K.A., Williams, M.E., Yaksh, T.L. Upregulation of dorsal root ganglion (alpha)2(delta) calcium channel subunit and its correlation with allodynia in spinal nerve-injured rats. *J Neurosci*, **2001**, *21*, 1868-1875.

[11]Davies, A., Hendrich, J., Van Minh, A.T., Wratten, J., Douglas, L., Dolphin, A.C. Functional biology of the $\alpha_2\delta$ subunits of voltage-gated calcium channels. *Trends Pharmacol Sci*, **2007**, *28*, 220-180.

[12]Marson, A.G., Al-Kharusi, A.M., Alwaidhi, M., Appleton, R., Baker, G.A., Chadwick, D.W., Cramp, C., Cockerell, O.C., Cooper, P.N., Doughty, J., Eaton, B., Gamble, C., Goulding, P.J., Howell, S.J., Hughes, A., Jackson, M., Jacoby, A., Kellett, M., Lawson, G. R., Leech, J.P., Nicolaides, P., Roberts, R., Shackley, P., Shen., J., Smith, D.F., Smith, P.E., Smith, C.T., Vanoli, A., Williamson, P.R. SANAD Study group. The SANAD study of effectiveness of carbamazepine, gabapentin, lamotrigine, oxcarbazepine, or topiramate for treatment of partial epilepsy: an unblinded randomised controlled trial. *Lancet*, **2007**, *369*, 1000-1015.

[13] Vranken, J.H. Mechanisms and treatment of neuropathic pain. *Cent Nerv Syst Agents Med Chem*, **2009**, *9*, 71-78.

[14] Thorpe, A.J., Offord, J. The alpha2-delta protein: an auxiliary subunit of voltage-dependent calcium channels as a recognized drug target. *Curr Opin Investig Drugs*, **2010**, *11*, 761-70.

[15]Jay, S.D., Sharp, A.H., Kahl, S.D., Vedvick, T.S., Harpold, M.M., Campbell, K.P. Structural characterization of the dihydropyridine-sensitive calcium channel α_2-subunit and the associated δ peptides. *J Biol Chem*, **1991**, *266*, 3287-3293.

[16]Calderón-Rivera, A., Andrade, A., Hernández-Hernández, O., Gonzalez-Ramirez, R., Sandoval, A., Rivera, M., Gomora, J.C., Felix, R. Identification of a disulfide bridge essential for structure and function of the voltage-gated Ca^{2+} channel $\alpha_2\delta$-1 auxiliary subunit. *Cell Calcium*, **2012**, *51*, 22-30.

[17]Wiser, O., Trus, M., Tobi, D., Halevi, S., Giladi, E., Atlas, D. The $\alpha_2\delta$ subunit of voltage-sensitive Ca^{2+} channels is a single transmembrane extracellular protein which is involved in regulated secretion. *FEBS Lett*, **1996**, *379*, 15-20.

[18]Robinson, P., Etheridge, S., Song, L., Shah, R., Fitzgerald, E.M., Jones, O.T. Targeting of voltage-gated calcium channel $\alpha_2\delta$-1 subunit to lipid rafts is independent from a GPI-anchoring motif. *PLoS One*, **2011**, *6*, e19802.

[19]Gurnett, C.A., De Waard, M., Campbell, K.P. Dual function of the voltage-dependent Ca^{2+} channel $\alpha_2\delta$ subunit in current stimulation and subunit interaction. *Neuron*, **1996**, *16*, 431-440.

[20]Gurnett, C.A., Felix, R., Campbell, K.P. Extracellular interaction of the voltage-dependent Ca^{2+} channel $\alpha_2\delta$ and a_1 subunits. *J Biol Chem*, **1997**, *272*, 18508-18512.

[21]Felix, R., Gurnett, C.A., De Waard, M., Campbell, K.P. Dissection of functional domains of the voltage-dependent Ca^{2+} channels $\alpha_2\delta$ subunit. *J Neurosci*, **1997**,*17*, 6884-6891.

[22] Kadurin, I., Alvarez-Laviada, A., Ng, S.F., Walker-Gray, R., D'Arco, M., Fadel, M.G., Pratt, W.S., Dolphin, A.C. Calcium currents are enhanced by α2δ-1 lacking its membrane anchor. *J Biol Chem* **2012**, *287*, 33554-33566.

[23]Whittaker, C.A., Hynes, R.O. Distribution and evolution of von Willebrand/Integrin A domains: Widely dispersed domains with roles in cell adhesion and elsewhere. *Molec Biol Cell*, **2002**, *13*, 3369-3387.

[24]Anantharaman, V., Aravind, L. Cache – a signaling domain common to animal Ca^{2+} channel subunits and a class of prokaryotic chemotaxis receptors. *Trends Biochem Sci*, **2000**, *25*, 535-537.

[25]Canti, C., Nieto-Rostro, M., Foucault, I., Heblich, F., Wratten, J., Richards, M.W., Hendrich, J., Douglas, L., Page, K.M., Davies, A., Dolphin, A.C. The metal ion dependent adhesion site in the Von Willebrand factor-A domain of $\alpha_2\delta$ subunits to key to trafficking voltage-gated Ca^{2+} channels. *Proc Natl Acad Sci USA*, **2005**, *102*, 11230-11235.

[26]Hoppa, M.B., Lana, B., Margas, W., Dolphin, A.C., Ryan, T.A. $\alpha_2\delta$ expression sets presynaptic calcium channel abundance and release probability. *Nature*, **2012**, *486*, 122-125.

[27] Gee, N.S., Brown, J.P., Dissanayake, V.U., Offord, J., Thurlow, R., Woodruff, G.N. The novel anticonvulsant drug gabapentin (Neurontin), binds to the $\alpha_2\delta$ subunit of a calcium channel. *J Biol Chem*, **1996**, *271*, 5768-5776.

[28]Hendrich, J., Van Minh, A.T., Heblich, F., Nieto-Rostro, M., Watschinger, K., Striessnig, J., Wratten, J., Davies, A., Dolphin, A.C. Pharmacological disruption of calcium channel trafficking by the $\alpha_2\delta$ ligand gabapentin. *Proc Natl Acad Sci USA*, **2008**, *105*, 3628-3633.

[29]Eroglu, C., Allen, N.J., Susman, M.W., O'Rourke, N.A., Park, C.Y., Ozkan, E., Chakraborty, C., Mulinyawe, S.B., Annis, D.S., Huberman, A.D., Green, E.M., Lawler, J., Dolmetsch, R., Garcia, K.C., Smith, S.J., Luo, Z.D., Rosenthal, A., Mosher, D.F., Barres, B.A. Gabapentin receptor $\alpha_2\delta$-1 is a neuronal Thrombospondin receptor responsible for excitatory CNS synaptogenesis. *Cell*, **2009**, *139*, 380-392.

[30]Wang, M., Offord, J., Oxender, D.L., Su, T.Z. Structural requirement of the calcium channel subunit $\alpha_2\delta$ for gabapentin binding. *Biochem J*, **1999**, *342*, 313-320.

[31] Cassidy, J.S., Ferron, L., Kadurin, I., Pratt, W.S., Dolphin, A.C. Functional exofacially tagged N-type calcium channels elucidate the interaction with auxiliary a2d-1 subunits. *Proc Natl Acad Sci USA,* **2014**, *111*, 8979-8984.

[32]McKeown, L., Robinson, P., Greenwood, S.M., Hu, W., Jones, O.T. PIN-G – a novel reporter for imaging and defining the effects of trafficking signals in membrane proteins. *BMC Biotechnol*, **2006**, *6*, 15 (epub).

[33]Geiser, M., Cèbe, R., Drewello, D., Schmitz, R. Integration of PCR fragments at any specific site within cloning vectors without the use of restriction enzymes and DNA ligase. *Biotechniques*, **2001**,*31*, 88-90, 92.

[34] Robinson, P., Etheridge, S., Song, L., Armenise, P., Jones, O.T., Fitzgerald, E.M. Formation of N-type ($Ca_v2.2$) voltage-gated calcium channel membrane microdomains: Lipid raft association and clustering. *Cell Calcium, **2010**, 48*, 183-194.

[35]Sandoval, A., Oviedo, N., Andrade, A., Felix, R. Glycosylation of asparagines 136 and 184 is necessary for the alpha2delta subunit-mediated regulation of voltage-gated Ca^{2+} channels. *FEBSLett*, **2004**, *576*, 21-26.

[36]Kinch, L., Yong Shi, S., Conq, Q., Cheng, H., Liao, Y., Grishin, N.V. CASP9 assessment of free modeling target predictions. *Proteins*, **2011**, *79 (Suppl 10)*, 59-73.

[37]Xu, D., Zhang, Y. Ab initio protein structure assembly using continuous structure fragments and optimized knowledge-based force field. *Proteins*, **2012**, *80*, 1715-1735.

[38] Dooley, D.J., Taylor, C.P., Donevan. S., Feltner, D. Ca^{2+} channel $alpha_2delta$ ligands: novel modulators of neurotransmission. *Trends Pharmacol Sci*, **2007**, *28*, 75-82.

[39] Pexton, T., Moeller-Bertram, T., Schilling, J.M., Wallace, M.S. Targeting voltage-gated calcium channels for the treatment of neuropathic pain: a review of drug development. *Expert Opin Investig Drugs*, **2011**, *20*, 1277-1284.

[40] Altier, C., Garcia-Caballero, A., Simms, B., You, H., Chen, L., Walcher, J., Tedford, H.W., Hermosilla, T., Zamponi, G.W. The $Ca_v\beta$ subunit prevents RFP2-mediated ubiquitination and preosomal degradation of L-type channels. *Nature Neurosci*, **2011**, *14*, 173 – 180.

[41] Tohse, N., Conforti, L., Sperelakis, N. BayK8644 enhances Ca^{2+} channel activities in embryonic chick heart cells without prolongation of open times. *Eur J Pharmacol*, **1991**, *201*, 307-310.

[42] Rampe, D., Anderson, B., Rapien-Pryor, V., L, T., Dage, R.C. Comparison of the in vitro and in vivo cardiovascular effects of two structurally distinct Ca^{2+} channel activators, BayK8644 and FPL 64176. *J Pharmacol Exp Ther*, **1993**, *265*, 1125-1130.

Figure Legends

Figure 1. The presence of the N-terminal R domain (residues 26-230) of $\alpha_2\delta$-1 is necessary for $\alpha_2\delta$-mediated modulation of $Ca_v2.2/\beta_{1b}$ currents. *A)* Structure of the PIN "head", and the rat wild type (WT) $\alpha_2\delta$-1 auxiliary subunit. Numbers indicate the boundaries for the α_2 and δ polypeptides, the documented Von Willebrand factor A (VWA) and Cache domains. The N-terminal region between the SP cleavage site and the VWA boundary is designated as the R domain. The sequence between the Cache domain and the $\alpha_2\delta$ cleavage boundary is split into two regions we designate as VGCC and Linker. All numbering is based on the full length $\alpha_2\delta$-1 polypeptide prior to cleavage of the signal peptide (SP, residues 1-25) in WT $\alpha_2\delta$-1 subunit. *(B)* Depiction of the PIN-$\alpha_2\delta$-1 domain chimera: PIN-TM (1061-1091), PIN-δ (948-1091), PIN-Linker (637-1091), PIN-VGCC (541-1091), PIN-Cache (436-1091), PIN-VWA (231-1091), PIN-$\alpha_2\delta$ (26-1091). *Inset*, PNGase-F deglycosylation assay for PIN-Cache, PIN-VWA and PIN-$\alpha_2\delta$ chimera. Constructs were separated by SDS-PAGE and immunoblotted against the external HA tag. Arrowheads indicate the band shifts due to deglycosylation. Approximate theoretical sizes for non-glycosylated constructs are as follows (in kDa): PIN-Cache, 78; PIN-VWA, 100; PIN-$\alpha_2\delta$, 124) *(C)* Average current density-voltage (*I-V)* plots for $Ca_v2.2/\beta_{1b}$ currents in the absence of $\alpha_2\delta$-1 (open circle) and in the presence of PIN-TM (closed square), PIN-δ (open square), PIN-Linker (closed triangle), PIN-Cache (closed diamond), PIN-VWA (open diamond) and full length PIN-$\alpha_2\delta$ (closed circle). Continuous lines indicate Boltzmann fits to *I-V* plots using the function described in the Methods. *(D)* Average steady state inactivation curves. Continuous lines represent curve fits using the function described in the Methods. Steady-state inactivation curves were obtained from individual cells using 100 ms duration test pulses to 20 mV, preceded by a 5s pre-pulse to potentials between -90 to +30 mV, from a holding potential, V_h, of –80 mV. *(E)* Representative peak current traces from cells expressing $Ca_v2.2/\beta_{1b}$ in the absence of $\alpha_2\delta$-1 and $Ca_v2.2/\beta_{1b}$ co-expressed with full length PIN-$\alpha_2\delta$ or PIN-VWA. Currents were evoked using 200 ms depolarizing steps in 5 mV intervals (-30 to +65 mV), from, V_h, -80 mV. All data are shown as the mean ± S.E.M., where cell number, *n,* is 9-18 for each construct.

Figure 2. The integrity of the N-terminal Rd-A region (residues 26-117) of $\alpha_2\delta$-1 is essential for $\alpha_2\delta$-mediated modulation of $Ca_v2.2/\beta_{1b}$ currents. *(A)* Subdivisions of the R domain and corresponding N-terminally extended PIN-$\alpha_2\delta$-1 chimera into regions A, B and C, based on inspection of the predicted secondary structure. Further sub-divisions (A1-A4, B1-B2, C1-C2 and A3a-d) were guided by experimentation. *(B)* Details of PIN-chimera extended towards the N-terminus by successive incorporation of the rat $\alpha_2\delta$-1 Rd sequences corresponding to the boundaries shown in *(A)* (numbering

based on full length un-processed $\alpha_2\delta$-1 polypeptide). *(C)* Average current density-voltage (*I-V)* plots for $Ca_v2.2/\beta_{1b}$ currents in the absence of $\alpha_2\delta$-1 (open circle) and in the presence of PIN-C1 (closed square), PIN-B1 (open square), PIN-A4 (closed triangle), PIN-dA3 (open triangle), PIN-cdA3 (closed diamond), PIN-bcdA3 (open diamond), PIN-A3 (closed star), PIN-A2 (open star) and full length PIN-$\alpha_2\delta$-1 (closed circle). Continuous lines indicate the Boltzmann fits to *I-V* plots using the function described in the Methods. *(D)* Representative peak current traces from cells expressing $Ca_v2.2/\beta_{1b}$ in the presence of selected PIN-chimera and PIN-$\alpha_2\delta$. Currents were evoked using 200 ms depolarizing steps in 5 mV intervals (-30 to +65 mV), from a holding potential, V_h, -80 mV. All data are shown as the mean ± S.E.M., where cell number, *n,* is 8-18 for each construct.

Figure 3. The N-terminal Rd alone is sufficient to restore fully the effects of $\alpha_2\delta$-mediated modulation of $Ca_v2.2/\beta_{1b}$ currents. *(A)* R domain chimera extended in the C-terminal direction. PIN chimera were extended towards the C-terminus by successive incorporation of the rat $\alpha_2\delta$-1 Rd sequences corresponding to the boundaries shown in Figure 2A. Constructs corresponding to a PIN-chimera containing the entire R domain (PIN-Rd) which replicates the biophysical effects of full length $\alpha_2\delta$-1 and functionally inactive mutants lacking 11 residues in C2 (PIN-Rd:Δ11) and the critical tryptophan W205 (PIN-Rd:W205A) are shown at bottom. *(B)* Average current density-voltage (*I-V)* plots for $Ca_v2.2/\beta_{1b}$ currents in the absence of $\alpha_2\delta$-1 (open circle) and in the presence of PIN-Rd-A (closed square), PIN-Rd-B1 (open square), PIN-Rd-B2 (closed triangle), PIN-Rd-C1 (open triangle), PIN-Rd (closed diamond) and full length PIN-$\alpha_2\delta$ (closed circle). *(C)* Representative peak current traces from cells expressing $Ca_v2.2/\beta_{1b}$ in the presence of PIN-Rd-C1 and PIN-Rd. *Inset*, representative PNGase-F deglycosylation assay of PIN-Rd (containing GFP+HA). The first three lines show migration in the absence of PNGase-F and in the absence (lane 1) or presence (lanes 2-3) of DTT. Lane 4 and arrowheads show the band shift with PNGase-F, indicating the presence of N-glycosylation sites [35]. *(D)* Average current density-voltage (*I-V)* plots for $Ca_v2.2/\beta_{1b}$ currents in the absence of $\alpha_2\delta$-1 (open circle) and in the presence of PIN- $\alpha_2\delta$-Δ11 (closed square), PIN-Rd-Δ11 (open square), PIN-Rd-W205A (closed triangle) and full length PIN-$\alpha_2\delta$ (closed circle). *(E)* Representative peak current traces from cells expressing $Ca_v2.2/\beta_{1b}$ in the presence of PIN-Rd-W205A and PIN-Rd-Δ11 compared with PIN-Rd and PIN-$_2\delta$-Δ11 compared with PIN-$\alpha_2\delta$. Currents were evoked using 200 ms depolarizing steps in 5 mV intervals (-30 to +65 mV), from a holding potential, V_h, -80 mV. All data are shown as the mean ± S.E.M., where cell number, *n*, is 9-20 for each construct.

Figure 4. Predicted tertiary structures of human wildtype and mutant (W205A) Rd-1 domain. Structures were generated using the *ab initio* protein folding and structure algorithm, QUARK

(http://zhanglab.ccmb.med.umich.edu/QUARK/). Structures are shown in side-on orientation with the major A1-2 and A3-4 helices at left. Colours correspond to inferred regions originally used in the structure-function analysis of rat Rd-1 (See Supp. Figs. S1 and S2) as follows: Rd-A: Light turquoise; Rd-B: lavender; Rd-C1: yellow; Rd-C2: light orange. The Region shown in C2 as dark orange corresponds to the core C2 residues (see Rd-1 Supp. Fig. S1), while the residue shown in red (asterisked) indicates the highly conserved tryptophan whose mutation to alanine in Rat Rd-1 abrogates function.

Table Legends

Table 1. Biophysical properties of $Ca_v2.2/\beta_{1b}$ channels co-expressed with different PIN-chimera. I_{max} is the maximum peak current density. Individual current density-voltage plots were fitted with a Boltzmann function: $I = (g(V-V_{rev}))/(1 + exp\ (1 – (V-V_{50,act})/k))$, where V_{rev} is the reversal potential, $V_{50,act}$ is the voltage for half maximal activation, k is the slope factor and g is conductance. % inact refers to percent inactivation of peak current after 500 ms. Statistically significant effects of PIN-chimera compared with control ($Ca_v2.2/\beta_{1b}$ currents in the absence of $\alpha_2\delta$, (-) $\alpha_2\delta$), were determined using Student's t-test and are denoted as follows: * $P < 0.05$, ** $P < 0.01$, *** $P < 0.001$. The number of cells per treatment is shown in parentheses. All data are shown as the mean ± S.E.M..

PIN chimera	I_{max} (pA.pF^{-1})	$V_{50,act}$ (mV)	k (mV)	% inact
(-) $\alpha_2\delta$	-14.8 ± 3.2 (14)	13.1 ± 1.8 (14)	4.7 ± 0.4 (14)	53 ± 6 (9)
PIN-$\alpha_2\delta$	-74.8 ± 8.3 (18) ***	6.3 ± 1.0 (18) ***	3.4 ± 0.3 (18) ***	76.9 ± 3.8 (11) **
PIN-TM	-14.6 ± 2.9 (12)	15.7 ± 1.1 (12)	5.3 ± 0.2 (12)	60.6 ± 9.4 (5)
PIN-δ	-12.0 ± 1.8 (12)	12.2 ± 1.4 (12)	5.1 ± 0.2 (12)	67.4 ± 4.9 (8)
PIN-Linker	-12.7 ± 3.8 (12)	13.7 ± 1.1 (12)	5.2 ± 0.2 (12)	59.1 ± 8.4 (7)
PIN-VGCC	-13.7 ± 2.2 (9)	13.8 ± 1.4 (9)	5.4 ± 0.1 (9)	60.2 ± 5.0 (6)
PIN-Cache	-14.9 ± 2.9 (13)	14.2 ± 0.9 (13)	5.5 ± 0.3 (13)	41.0 ± 6.0 (8)
PIN-VWA	-15.8 ± 1.8 (17)	15.3 ± 0.9 (17)	5.1 ± 0.2 (17)	53.8 ± 6.3 (9)
PIN-C1	-12.1 ± 1.6 (14)	12.9 ± 1.6 (14)	5.4 ± 0.2 (14)	48.8 ± 8.0 (10)
PIN-B1	-16.4 ± 2.6 (11)	10.1 ± 0.7 (11)	5.1 ± 0.1 (14)	47.4 ± 7.7 (10)
PIN-A4	-15.4 ± 1.8 (11)	10.3 ± 0.5 (11)	5.1 ± 0.3 (11)	69.7 ± 3.4 (11)
PIN-A3d	-28.4 ± 3.6 (10)	8.2 ± 1.0 (10) **	4.4 ± 0.3 (10)	61.5 ± 5.3 (6)
PIN-A3cd	-27.5 ± 2.8 (8)	7.4 ± 2.0 (8) **	4.6 ± 0.2 (8)	69.4 ± 7.0 (8)
PIN-A3bcd	-39.1 ± 4.2 (11)	5.8 ± 1.0 (11) ***	4.0 ± 0.2 (11)	60.5 ± 8.0 (7)
PIN-A3	-58.8 ± 9.8 (12) ***	2.9 ± 0.7 (12) ***	3.4 ± 0.3 (12) ***	57.9 ± 4.6 (13)
PIN-A2	-72.7 ± 10.2 (13) ***	4.5 ± 0.7 (13) ***	3.6 ± 0.3 (13) **	79.9 ± 3.4 (11) **
PIN-RdA	-26.4 ± 8.2 (15)	12.4 ± 1.7 (15)	4.8 ± 0.3 (15)	57.9 ± 8 (11)
PIN-RdB1	-16.4 ± 2.6 (9)	14.0 ± 1.9 (9)	5.1 ± 0.5 (9)	63.1 ± 10.1 (6)
PIN-RdB	-20.8 ± 4.7 (9)	10.3 ± 2.3 (9)	5.4 ± 0.4 (9)	65.0 ± 8.3 (8)
PIN-RdC1	-17.5 ± 2.6 (10)	10.0 ± 1.3 (10)	4.9 ± 0.4 (10)	65.8 ± 9.1 (6)
PIN-Rd	-73.4 ± 7.5 (20) ***	6.7 ± 0.9 (20) **	3.2 ± 0.2 (20) ***	86.6 ± 4.0 (9) ***
PIN-Rd:Δ11	-11.4 ± 1.9 (16)	10.7 ± 1.0 (16)	5.7 ± 0.3 (16) **	79.5 ± 5.1 (11) ***
PIN-Rd:W205A	-11.7 ± 3.1 (12)	11.1 ± 1.5 (12)	6.2 ± 0.3 (12) **	80.9 ± 3.6 (10) ***
PIN-$\alpha_2\delta$:Δ11	-13.4 ± 2.2 (18)	10.7 ± 1.0 (18)	5.7 ± 0.3 (18) *	76.4 ± 3.8 (7) **

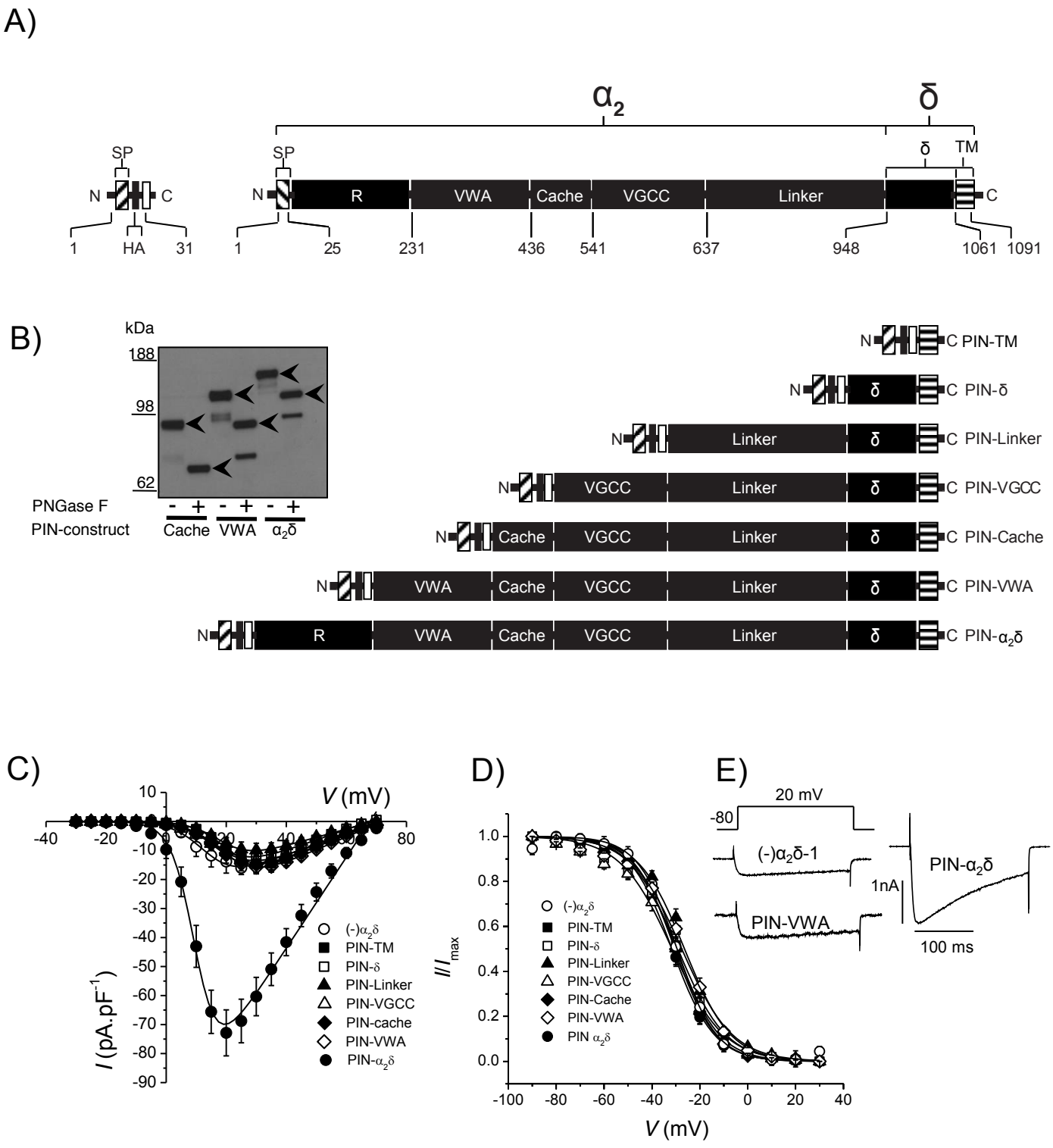
A)
α2
δ
SP
N
C
HA
1
31
R
VWA
Cache
VGCC
Linker
TM
25
231
436
541
637
948
1061
1091
B)
kDa
188
98
62
PNGase F
PIN-construct
Cache
VWA
α2δ
PIN-TM
PIN-δ
PIN-Linker
PIN-VGCC
PIN-Cache
PIN-VWA
PIN-α2δ
C)
V (mV)
I (pA.pF-1)
(-)α2δ
PIN-TM
PIN-δ
PIN-Linker
PIN-VGCC
PIN-cache
PIN-VWA
PIN-α2δ
D)
I/Imax
V (mV)
PIN α2δ
E)
20 mV
-80
(-)α2δ-1
PIN-VWA
PIN-α2δ
1nA
100 ms

Fig. 1

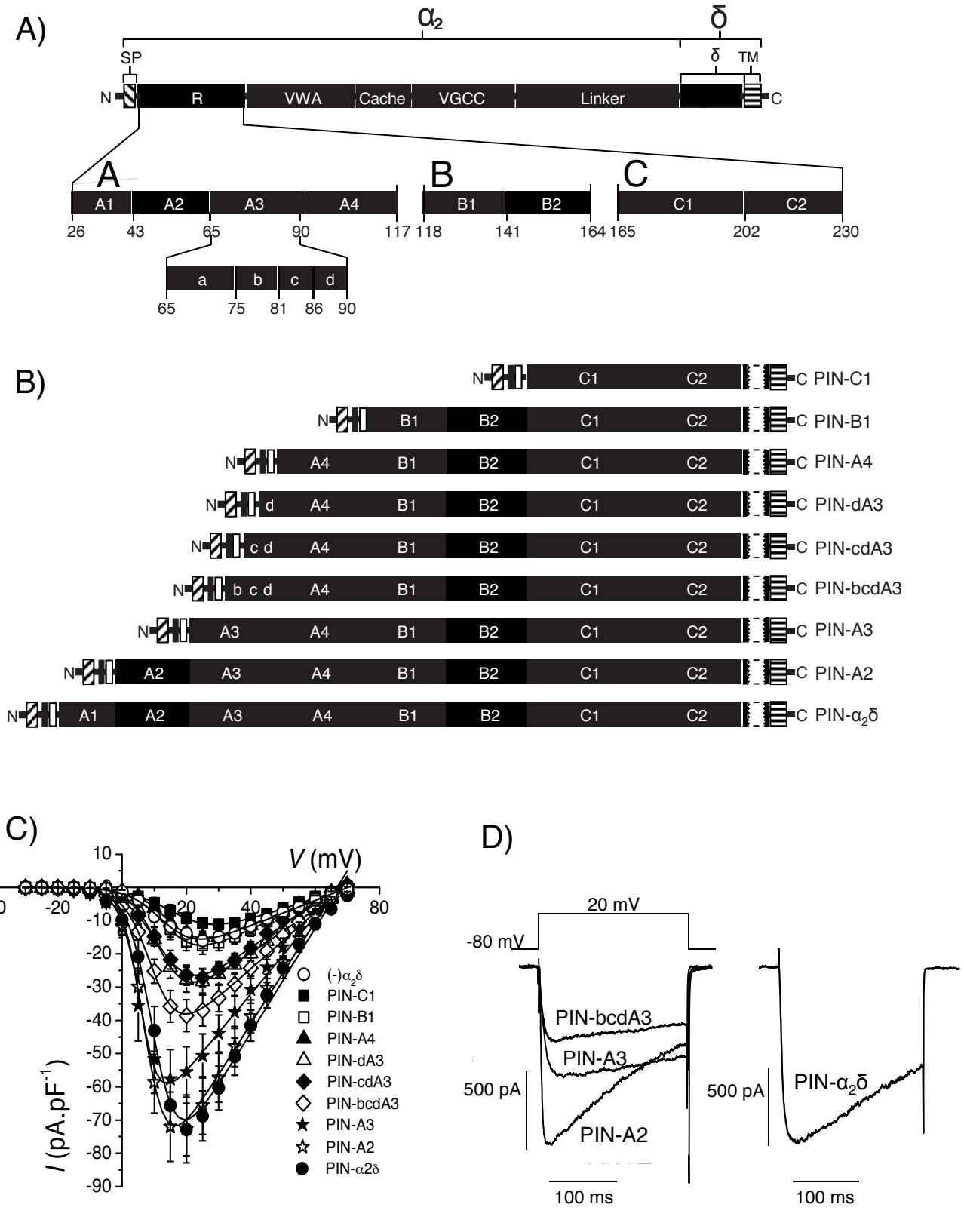
A)
α2
δ
SP
δ
TM
N
R
VWA
Cache
VGCC
Linker
C
A
B
C
A1
A2
A3
A4
B1
B2
C1
C2
26
43
65
90
117
118
141
164
165
202
230
a
b
c
d
65
75
81
86
90
B)
PIN-C1
PIN-B1
PIN-A4
PIN-dA3
PIN-cdA3
PIN-bcdA3
PIN-A3
PIN-A2
PIN-α2δ
C)
V (mV)
I (pA.pF-1)
(-)α2δ
PIN-C1
PIN-B1
PIN-A4
PIN-dA3
PIN-cdA3
PIN-bcdA3
PIN-A3
PIN-A2
PIN-α2δ
D)
20 mV
-80 mV
PIN-bcdA3
PIN-A3
PIN-A2
500 pA
100 ms
PIN-α2δ
500 pA
100 ms

Fig. 2

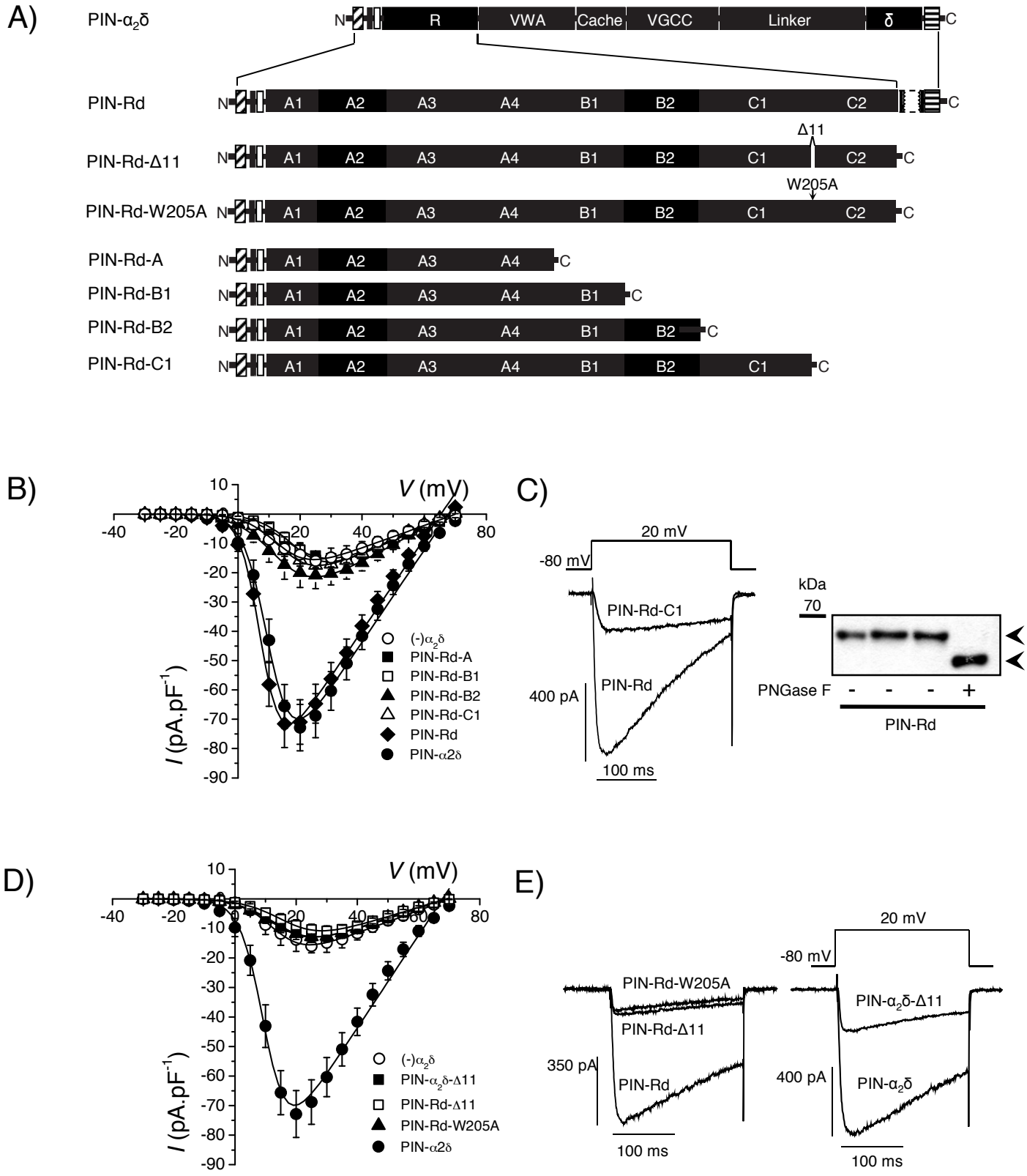
A)
PIN-α2δ
N
R
VWA
Cache
VGCC
Linker
δ
C
PIN-Rd
A1
A2
A3
A4
B1
B2
C1
C2
PIN-Rd-Δ11
Δ11
PIN-Rd-W205A
W205A
PIN-Rd-A
PIN-Rd-B1
PIN-Rd-B2
PIN-Rd-C1
B)
V (mV)
I (pA.pF-1)
(-)α2δ
PIN-Rd-A
PIN-Rd-B1
PIN-Rd-B2
PIN-Rd-C1
PIN-Rd
PIN-α2δ
C)
20 mV
-80 mV
PIN-Rd-C1
PIN-Rd
400 pA
100 ms
kDa
70
PNGase F
PIN-Rd
D)
V (mV)
I (pA.pF-1)
(-)α2δ
PIN-α2δ-Δ11
PIN-Rd-Δ11
PIN-Rd-W205A
PIN-α2δ
E)
20 mV
-80 mV
PIN-Rd-W205A
PIN-Rd-Δ11
PIN-Rd
350 pA
100 ms
PIN-α2δ-Δ11
PIN-α2δ
400 pA
100 ms

Fig. 3

A)

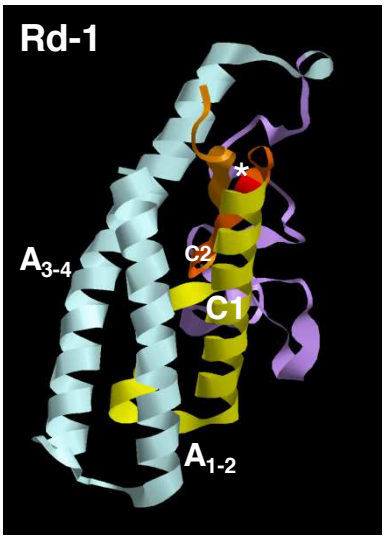

B)

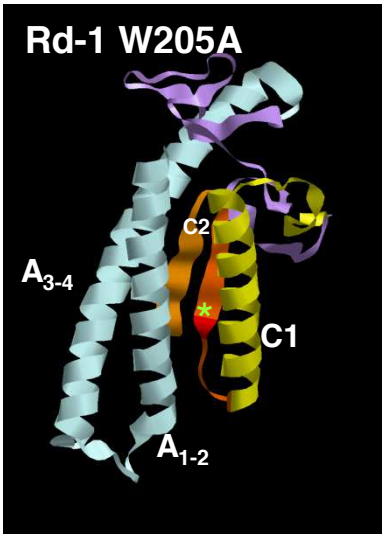

Fig. 4

Supplementary Figure Legends

Supp. Fig. S1. Comparison of the R domain sequences of the $\alpha_2\delta$-1 to -4 subunits. Sequences of the R domains of $\alpha_2\delta$-1 to -4 (Human Rd-1-4; assigned using Archaeopteryx (See Legend Supp. Fig. 4)), were aligned and the degree of residue conservation (consistency) at each position determined using the PRALINE software package (http://www.ibi.vu.nl/programs/pralinewww/). For reference and display purposes, the degree of consistency determined for each R domain dataset is shown below the relevant human sequence. All numbering is based on the position of residues displayed upon alignment. Also shown are the Rd-A, -B and -C regions (bounded by large vertical ticks) within Rd-1 (See Fig. 1) and their inferred counterparts in Rds-2 to -4. The line under Rd-1 positions 179-189 (corresponding to 200-210 in rat Rd-1) denotes the core Rd-C2 residues deleted in the PIN-Rd-Δ11 construct. The conserved tryptophan (W205 in rat Rd-1) is denoted by an inverted triangle. Note the high degree of conservation, especially in Rd-C and, to a lesser extent, Rd-A regions within each Rd.

Supp. Fig. S2. Comparison of predicted R domain tertiary structures. Structures inferred for the human R domains, Rd-1, Rd-2, -3 and -4 are shown. Each structure was generated using the *ab initio* protein folding and structure algorithm, QUARK (http://zhanglab.ccmb.med.umich.edu/QUARK/). All structures are shown in side-on orientation with the major A1-2 and A3-4 helices at left. Colours correspond to inferred regions originally used in the structure-function analysis of rat Rd-1 (See Supp. Figs. S1 and S2) as follows: Rd-A: Light turquoise; Rd-B: lavender; Rd-C1: yellow; Rd-C2: light orange. The Region shown in C2 as dark orange corresponds to the core C2 residues (see Rd-1 Supp. Fig. S1), while the residue shown in red (asterisked) indicates the highly conserved tryptophan whose mutation to alanine in Rat Rd-1 abrogates function. Although the order of the A1-2 and A3-4 helices and the orientation of the C2 residues can differ, all predicted structures show a common theme where Rd-C2 residues form a "tongue", buried under a partial coiled-coil formed by the Rd-A region and Rd-C1 helix with infill provided by the least conserved Rd-B region.

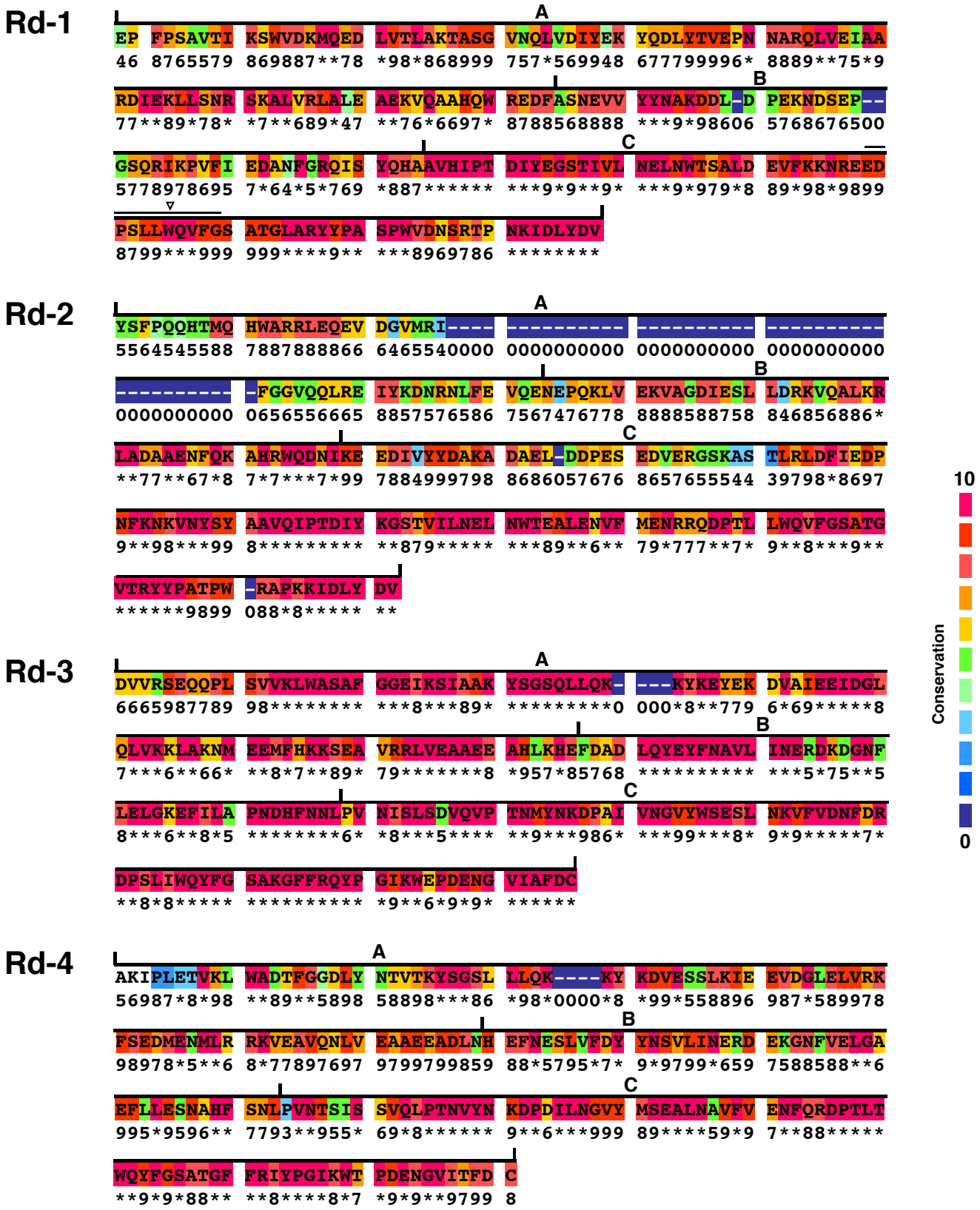

Supp. Fig. 1

Supp Fig 2.

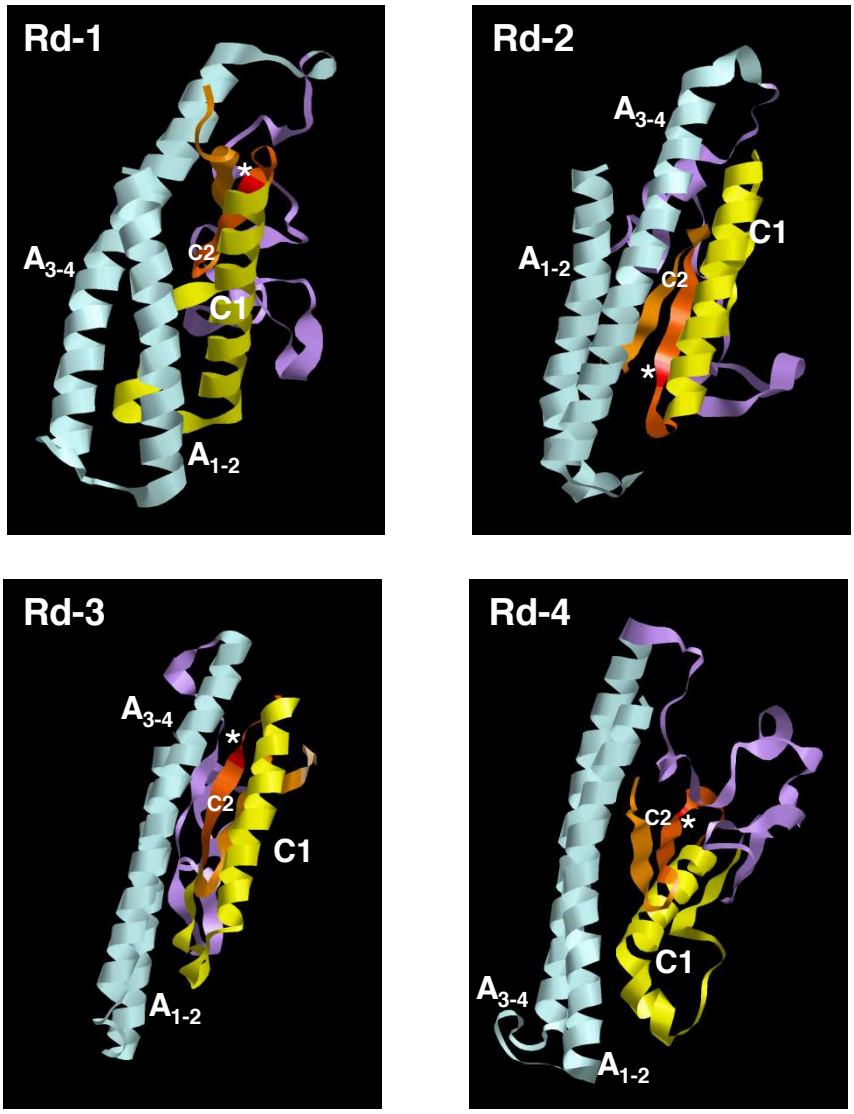
Rd-1
A3-4
C2
C1
A1-2
Rd-2
A3-4
C1
A1-2
C2
*
Rd-3
A3-4
*
C2
C1
A1-2
Rd-4
C2
*
C1
A3-4
A1-2